Cerdá, Sandra López; Fontana, Flavia; Wang, Shiqi; Correia, Alexandra; Molinaro, Giuseppina; Tello, Rubén Pareja; Hirvonen, Jouni; Celia, Christian; Barreto, Goncalo; Santos, Hélder A.

Development of siRNA and Budesonide Dual-Loaded Hybrid Lipid–Polymer Nanoparticles by Microfluidics Technology as a Platform for Dual Drug Delivery to Macrophages : An In Vitro Mechanistic Study

Published in:
Advanced Therapeutics

DOI:
10.1002/adtp.202300048

Published: 01/08/2023

Document Version
Publisher's PDF, also known as Version of record

ADVANCED THERAPEUTICS
www.advtherap.com

Development of siRNA and Budesonide Dual-Loaded Hybrid Lipid–Polymer Nanoparticles by Microfluidics Technology as a Platform for Dual Drug Delivery to Macrophages: An In Vitro Mechanistic Study

*Sandra López Cerdá, Flavia Fontana, Shiqi Wang, Alexandra Correia, Giuseppina Molinaro, Rubén Pareja Tello, Jouni Hirvonen, Christian Celia, Goncalo Barreto, and Hélder A. Santos**

Macrophages play a key role in the development of many diseases, like tissue injury, cancer, and autoimmune diseases. So far, single-drug loaded nanoparticles are developed to target macrophages. Nevertheless, macrophage dysregulation can induce multiple conditions, i.e., inflammation and fibrosis. Therefore, the simultaneous codelivery of a small molecule drug and a small interfering RNA (siRNA) for gene silencing may be beneficial to modulate macrophage dysfunction. Herein, hybrid lipid–polymer nanoparticles (LPNs) coloaded with both budesonide and enhanced green fluorescence protein siRNA (eGFP-siRNA) as model anti-inflammatory small molecule drug and siRNA, respectively, are developed by an optimized microfluidics method. Specifically, a poly(lactic-*co*-glycolic acid) core is coated by a lipid shell, and LPNs with size homogeneity and colloidal stability are obtained. Both payloads are loaded efficiently, and a controlled release is achieved. Additionally, LPNs are nontoxic in murine RAW 264.7 cells and human THP-1 cells and are efficiently taken up by these cells. Finally, the transfection efficiency of dual-loaded LPNs is high at low LPNs doses, thus proving the suitability of this nanosystem for gene silencing. Overall, the optimized LPNs are a suitable nanoplatform for the dual drug delivery to macrophages for the treatment of complex conditions requiring dual therapeutic approaches.

1. Introduction

Macrophages are immune cells involved in the maintenance of the normal homeostasis of the tissues and in keeping proper organ function, but also act as a double-edge sword in the development of many diseases, such as cancer, autoimmune diseases, and tissue injury.[1–3] The plasticity of macrophages makes them susceptible to chemical and biological cues in the surrounding environment, changing their phenotypes and functions accordingly.[3] The switch of phenotypes and functions is beneficial in self-limiting immune-responses, but also poses significant threats to normal tissues, for example, in the case of aberrant resolution of inflammation or in the case of fibrosis due to unpaired tissue regeneration.[1]

Alongside the fast advance of the nanomedicine field in the last years, nanoparticle (NP)-based approaches, such as dendrimers, polymeric, lipidic or inorganic NPs, have been developed to tackle

S. L. Cerdá, F. Fontana, S. Wang, A. Correia, G. Molinaro, R. P. Tello, J. Hirvonen, H. A. Santos
Drug Research Program
Division of Pharmaceutical Chemistry and Technology
University of Helsinki
Helsinki FI-00014, Finland
E-mail: h.a.santos@umcg.nl

The ORCID identification number(s) for the author(s) of this article can be found under https://doi.org/10.1002/adtp.202300048

DOI: 10.1002/adtp.202300048

C. Celia
Department of Pharmacy
University of Chieti – Pescara "G. d'Annunzio"
Via dei Vestini 31, Chieti I-66100, Italy

C. Celia
Laboratory of Drug Targets Histopathology
Institute of Cardiology
Lithuanian University of Health Sciences
A. Mickeviciaus g. 9, Kaunas LT-44307, Lithuania

G. Barreto
Translational Immunology Research Program
Faculty of Medicine, University of Helsinki
PL 4 (Yliopistonkatu 3), Helsinki 00014, Finland

G. Barreto
Orton Orthopedic Hospital, Tenholantie 10
Helsinki 00280, Finland

one of the different aspects of macrophage disfunction, such as inflammation, fibrosis, or tumorigenesis.[4–8] Nevertheless, certain conditions, such as tissue injury, require dual therapeutic approaches that tackle several aspects of macrophage dysfunction to achieve therapeutic success.[1,9,10] For instance, in the context of tissue injury, macrophages participate in the different stages of the tissue regeneration process. At initial stages, macrophages produce inflammatory mediators and growth factors and degrade the extracellular matrix (ECM), while at later stages, they must assume an anti-inflammatory role leading to the resolution of inflammation and the formation of a permanent collagenous matrix.[1] Nevertheless, dysregulated macrophage function after tissue injury can cause a prolonged exposure to proinflammatory stimuli and can lead to the development of scar tissue and pathological fibrosis, hampering complete recovery of tissue function.[11] Hence, many NPs have aimed to target macrophages by delivering a single drug molecule to inhibit either inflammation or fibrosis for tissue regeneration.[12] Nonetheless, both conditions should be tackled to achieve complete tissue repair.[13] This example highlights that is essential to develop dual drug-loaded NPs to modulate macrophages for the treatment of complex conditions like tissue injury, for which dual therapeutic approaches based on nanomedicine have not been reported so far.

Recently, studies have combined the advantages of both lipid and polymer NPs by designing hybrid lipid–polymer NPs (LPNs).[14–17] On the one hand, lipid NPs have been proven to be safe and efficient nanocarriers for gene delivery, as evidenced by the approval of Onpattro (patisiran) and the mRNA-1273 and BNT162b2 COVID-19 vaccines.[18] Typically, lipid NPs are composed of ionizable cationic lipids, cholesterol, phospholipids, and in some cases, poly(ethylene glycol) (PEG)–lipids.[19] As a result of the research concerning the design of novel cationic lipids, lipid NPs can now achieve high levels of transfection efficiency using nontoxic lipid NP doses.[20] On the other hand, polymeric NPs have been extensively used for the loading of hydrophobic small molecule drugs with high loading degrees, allowing to fine-tune the release profile according to the characteristics of the polymer.[21,22] Specifically, poly(lactic-*co*-glycolic acid) (PLGA) is a Food and Drug Administration (FDA) approved biodegradable polymer that has been extensively used to formulate PLGA NPs. Due to its biocompatibility and tuneable mechanical properties, it has been used for the controlled release of a wide variety of payloads with different applications.[23] Besides, some PLGA-based nanocarriers have already reached the clinic, such as antigen-loaded PEG–PLGA NPs to treat prostate cancer.[24] As a result of the combination of the previously mentioned lipids and polymer, LPNs have been formulated to render NPs with a core–shell structure consisting of a polymeric core coated by a lipid layer. This unique structural design provides desirable properties to the nanocarrier, since it guarantees high structural integrity and biocompatibility, enhanced interaction with cell membranes, storage stability, and controllable release kinetics.[14]

It has also been stated that one of the main advantages of LPNs is the possibility to load two different drugs to render a dual therapeutic effect.[15] Compared to lipid or polymeric NPs, LPNs can potentially load cargoes with different physicochemical properties, i.e., hydrophilicity and molecular weight. In addition, LPNs have the potential to load both cargos with higher efficiencies, since the two drugs are not loaded in the same NP compartment.[25] So far, several bulk methods have been reported for the formulation of LPNs, being the double-emulsion solvent evaporation technique the most common one to achieve high encapsulation efficiencies (EEs).[15] Nevertheless, microfluidics technology offers advantages over the conventional bulk methods, such as the higher EE of payloads, narrower size distribution of the particles, colloidal stability, and the possibility to scale-up the fabrication method.[26] In this context, some studies have used microfluidics to fabricate LPNs,[27] but very few examples can be found concerning the coloading of two cargos in LPNs through microfluidics,[28] particularly when it comes to combining small molecule drugs and nucleic acids, such as small interfering RNAs (siRNAs).[29]

In this work, LPNs coloaded with budesonide (BUD) and an enhanced green fluorescence protein (eGFP) siRNA as model small molecule drug and siRNA, respectively, were developed by a newly optimized microfluidics method as a platform for dual drug delivery to macrophages. LPNs composed of a PLGA core coated by a lipid layer were prepared by a two-steps coflow microfluidics method using in-house manufactured nanoprecipitation chips.[30–34] In the first microfluidics step, BUD was loaded into the PLGA core as a model small molecule drug, since it is an FDA-approved hydrophobic drug that can be used in many applications to reduce inflammation.[35,36] In the second microfluidic step, eGFP-siRNA was loaded in a lipid shell, since eGFP-siRNA is a model siRNA that can be used in preliminary studies to optimize the formulation parameters and acts as a surrogate of potential siRNAs against disease-related genes.[37] The size and morphology of the optimized LPNs were characterized by dynamic light scattering (DLS) and transmission electron microscopy (TEM). The in vitro drug release of budesonide and eGFP-siRNA was evaluated, and the cytotoxicity, cellular uptake, and cellular uptake mechanisms were tested on murine macrophages (RAW 264.7) and human THP-1 cells differentiated to macrophages. Finally, the siRNA transfection efficiency was also evaluated in eGFP-expressing RAW 264.7 cells to confirm the ability of the nanocarrier to escape the endosome and silence the expression of the targeted gene.

G. Barreto
Medical Ultrasonics Laboratory (MEDUSA)
Department of Neuroscience and Biomedical Engineering
Aalto University
Espoo 02150, Finland

H. A. Santos
Department of Biomedical Engineering
University Medical Center Groningen
University of Groningen
Ant. Deusinglaan 1, Groningen 9713 AV, The Netherlands

H. A. Santos
W.J. Kolff Institute for Biomedical Engineering and Materials Science
University Medical Center Groningen
University of Groningen
Ant. Deusinglaan 1, Groningen 9713 AV, The Netherlands

2. Results and Discussion

2.1. Nanoparticle Preparation and Physicochemical Characterization

Empty and dual drug-loaded LPNs were fabricated by a newly optimized two-steps microfluidics method using a nanoprecipitation process. For this purpose, in-house microfluidics chips were fabricated based on a previously described method and chip design.[26,38]

Optimizing microfluidics process parameters and formulation parameters is essential for the development of a reproducible method and the production of NPs with suitable physicochemical properties.[39] Hence, several optimizations were carried out in the first and second steps of this microfluidics approach.

In the first step, when the PLGA core is obtained, the concentration of PLGA in the organic phase, the flow rates and the polyvinyl alcohol (PVA) content were optimized sequentially to have PLGA cores below 250 nm and polydispersity index (PDI) < 0.2, and hybrid LPNs below 500 nm with PDI < 0.25 (**Figure 1**A; Tables S1–S4, Supporting Information).

In the second step of the microfluidics approach, when the PLGA core is coated by a lipid shell (Figure 1A), the selection of the type of lipids (cKK-E12, cholesterol, and 1,2-distearoyl-sn-glycero-3-phosphocholine (DSPC)) and of their molar ratio of 50:10:38.5 was based on previous works.[40] DSPC was chosen as optimal helper lipid instead of DOPE because it has been proved to be more suitable for siRNA delivery, while the cKK-E12 cationic lipidoid was used for siRNA complexation. In contrast to the commonly used cationic lipids, like dioleoyl-3-trimethylammonium propane, lipidoids contain several secondary and tertiary amines, which render these lipids more efficient in interacting with nucleic acids without significantly increasing the net charge of the NP, thus preventing toxicity.[41] Other formulation parameters, like the PLGA:lipids weight ratio and the cKK-E12 lipid:siRNA weight ratio, were optimized based on the siRNA EE data, as given in Section 2.2.

After preparation, the NPs were characterized by DLS to obtain information about their size (nm), PDI, and ζ-potential (Figure 1). After optimization of the first microfluidic step, a PLGA concentration of 5 mg mL^{-1} was selected for the organic phase, a 1% PVA concentration was selected for the aqueous phase and a flow rate ratio of 3:90 mL h^{-1} was selected for the organic and aqueous phases, respectively (Tables S1–S4, Supporting Information). The PLGA cores showed a size of 240 nm, which allows to keep the average size below 500 nm after coating with the lipid mixture (Figure 1B,C). The PDI of the PLGA core was 0.11, which ensures the particles homogeneity for the next microfluidics step. The particle charge was −23 mV, which is characteristic of PLGA NPs.[42] After coating with the lipid shell, the resulting empty LPNs had a size of 320 nm and a PDI of 0.19 (Figure 1B,C). The increase in the size and the PDI with respect to the PLGA core is expectable due to the presence of the lipid shell wrapping the PLGA core. The size of LPNs is suitable for local administration via either subcutaneous or intramuscular route, and the narrow size distribution, as well as the net positive charge over +20 mV, confirms the colloidal stability of the final formulation.

In addition, the fact that the particle charge becomes positive (+24 mV) confirms the presence of the lipid shell coating completely the PLGA core. This surface charge agrees with data previously reported for the cKK-E12 cationic lipidoid,[43] and explains that LPNs are stable due to electrostatic repulsion forces. Since the optimized LPNs are colloidally stable, no PEG was added, as it is commonly done for other lipid NPs formulations.[44] This is advantageous because it reduces the number of components in the formulation, thus reducing the costs and the complexity of the system, increasing its potentiality for the scale-up fabrication, and most importantly, avoiding the possible immunogenicity associated to the production of anti-PEG antibodies that is currently discussed in the literature.[45] When LPNs were loaded with BUD in the PLGA core (BUD@LPNs) or with eGFP-siRNA in the lipid shell (siRNA@LPNs), and when they were loaded with both (BUD@siRNA@LPNs), the size and PDI did not vary significantly, confirming that the loading of one or both cargoes does not affect the physicochemical properties of the optimized LPNs (Figure 1B,C).

The morphology and shape of NPs were also evaluated by TEM. In Figure 1C and Figure S1 (Supporting Information), single particle images and multiple particles TEM images, respectively, are displayed. PLGA cores, empty LPNs, single-loaded and dual-loaded LPNs had a round shape, with sizes smaller than the ones measured in DLS. This phenomenon can be explained by the fact that TEM allows to evaluate the size of the "dry" particles, while the DLS analysis measures the hydrodynamic diameter, which considers the water layer surrounding the particles.[46] Furthermore, DLS measures the size distribution within a particle population, and as shown in the graphs of the percentages of intensity in Figure 1C, the size of the particles follows a Gaussian distribution ranging from 150 to ≈800 nm; in TEM we are observing one or multiple particles but they are not representative of the entire population.

In vitro studies were carried out in cell culture medium, and the stability of NPs may be affected by the complex components of cell culture medium. Hence, the colloidal stability of LPNs versus the PLGA core was determined in the cell culture mediums of RAW 264.7 cells and THP-1 cells, since these are the cell lines used in this work. As shown in **Figure 2**A–C, PLGA NPs are stable in both cell culture media until 24 h, since no remarkable increase on the size or the PDI is observed. It should be noted that LPNs show an increase in the size at 5 and 15 min, and the PDI increases slightly in Dulbecco's Modified Eagle Medium (DMEM), but it is never above 0.35, thus meaning that the particles show acceptable colloidal stability even when interacting with the components of the cell culture mediums (Figure 2D,F). Additionally, as it has been reported previously,[31] the ζ-potential of both PLGA NPs and LPNs in cell culture medium is close to −12 mV, due to the effect of protein opsonization around the particles, which affects their overall charge distribution and interface properties.

In addition, the colloidal stability of PLGA NPs versus LPNs was also evaluated in sucrose 5.4% (w/v), since this is a common vehicle used for NPs administration. Both PLGA NPs and LPNs are colloidally stable in sucrose since no remarkable increase in size or PDI is recorded (Figure 2A,B,D,E). Besides, the ζ-potential of the fresh formulations does not change in sucrose

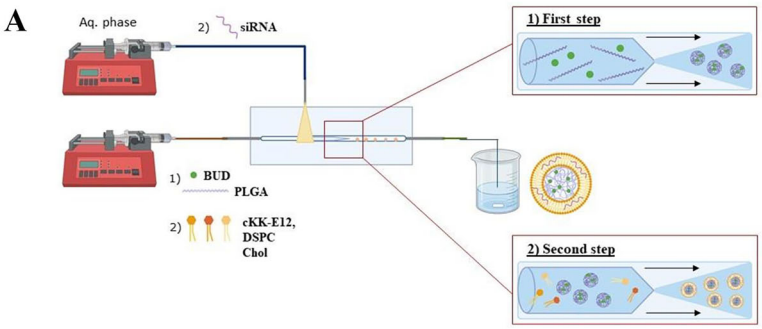

B

NPs label	Size (nm)	PDI	ζ-potential (mV)
PLGA core	240 ± 6	0.11 ± 0.07	-23 ± 2
Empty LPNs	320 ± 8	0.19 ± 0.08	+25 ± 1
BUD@LPNs	341 ± 6	0.2 ± 0.03	+24.6 ± 3
siRNA@LPNs	340 ± 4	0.22 ± 0.05	+25.2 ± 1
BUD@siRNA@LPNs	345 ± 7	0.22 ± 0.09	+25 ± 1

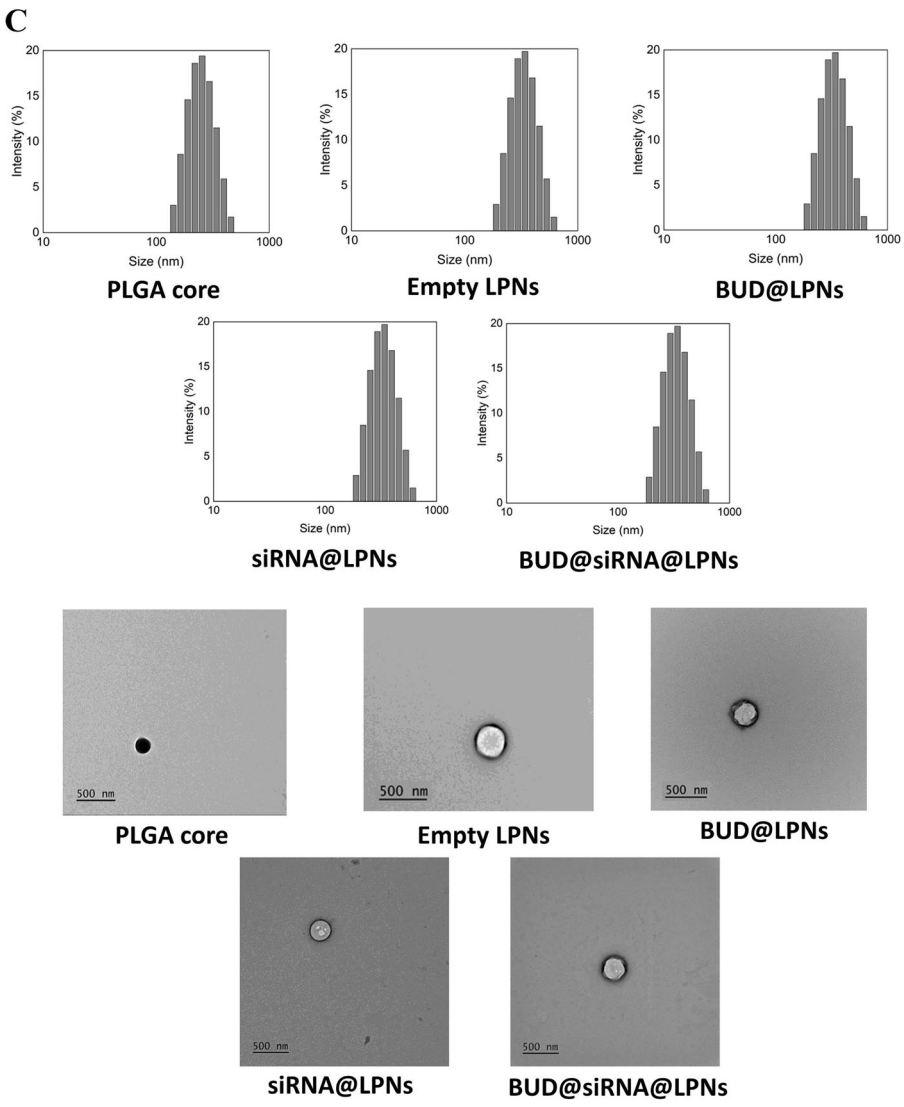

(Figure 2C,F). This effect was different from what was observed in cell culture medium because in sucrose there is no opsonization effect that occurs when particles are dispersed in cell culture medium.[47]

2.2. EE and Loading Degree (LD) of LPNs

Due to the highly hydrophobicity of BUD and the hydrophilicity of nucleic acids, BUD was encapsulated into the PLGA core by dissolving the drug in acetone in the first microfluidic step, while the siRNA was dissolved in nuclease-free PVA in the second microfluidics step (Figure 1A), in order to prevent degradation of the molecule during the preparation of LPNs. After purification, LPNs were washed four times to remove as much as possible the drug adsorbed to the NP surface. BUD in LPNs was quantified by using a previously optimized high performance liquid chromatography (HPLC) method upon releasing the drug from the PLGA core by mixing 500 µg of NPs with 3:2 (v/v) acetonitrile (ACN):dimethyl sulfoxide (DMSO).[48] The external calibration curve is shown in Figure S2A of the Supporting Information. The loading degree (LD) of BUD was calculated for optimization purposes. Interestingly, the LD of BUD in the PLGA cores was different depending on the initial amount of drug added during the experimental design of NPs. When 1 mg of BUD was loaded in 5 mg of PLGA NPs, the LD was 1.6% (**Figure 3**A), in agreement with previous reports loading BUD in polymeric NPs by microfluidics.[35] This LD is enough to produce an effect on cells.[49] However, when 2.5 mg of BUD was loaded in 5 mg of PLGA NPs, the LD was 18.2% (Figure 3A). The increase in the LD when the initial amount of BUD added is increased has been previously reported, and can be explained by the fact that when higher amounts of BUD are added, there are more hydrophobic interactions between the PLGA core and the drug.[49] Nevertheless, when 5 mg of BUD was loaded into 5 mg of PLGA core, an LD of 17.9% was obtained, similar to the LD obtained when 2.5 mg BUD was added. This suggests that there is a limit in the BUD that can be loaded inside PLGA NPs, and this limit depends

Figure 1. Physicochemical characterization of the optimized empty and dual drug-loaded LPNs. A) Schematic representation of the optimized two steps coflow microfluidics approach to produce dual drug-loaded LPNs. In the first step, BUD and PLGA are dissolved in the organic phase (acetone) and are mixed with the aqueous phase containing PVA to render BUD@PLGA NPs. In the second step, the prepared BUD@PLGA NPs are resuspended in ethanol and the lipids cKK-E12, DSPC, and cholesterol are dissolved in this organic phase. The siRNA is dissolved in the aqueous phase containing PVA and upon rapid mixing of both phases, the siRNA is complexed by the lipids, which wrap the BUD@PLGA core rendering BUD@siRNA@LPNs. B) Average size, PDI, and ζ-potential of the empty PLGA core, empty LPNs, BUD@LPNs, siRNA@LPNs, and BUD@siRNA@LPNs as measured by DLS. Values are represented as the mean ± standard deviation (s.d.) ($n = 3$). C) DLS intensity distribution profiles and TEM images of PLGA NPs, empty LPNs, BUD@LPNs, siRNA@LPNs, and BUD@siRNA@LPNs, respectively. Scale bars are shown in the images.

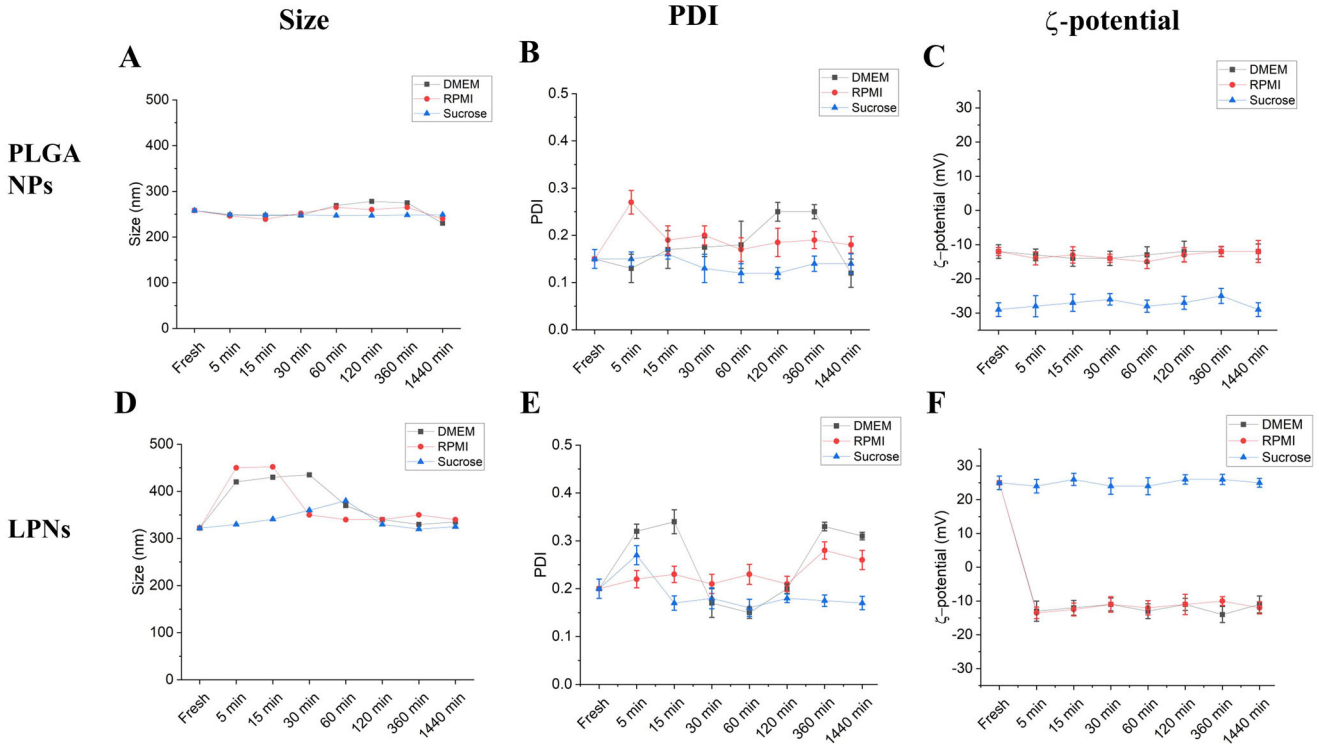

Figure 2. Evaluation of the colloidal stability of PLGA NPs versus LPNs in different media at 37 °C. Stability studies were performed by A,D) recording size, B,E) PDI, and C,F) ζ-potential in supplemented DMEM and RPMI cell culture mediums and sucrose 5.4%. Values are represented as the mean ± s.d. ($n \geq 3$).

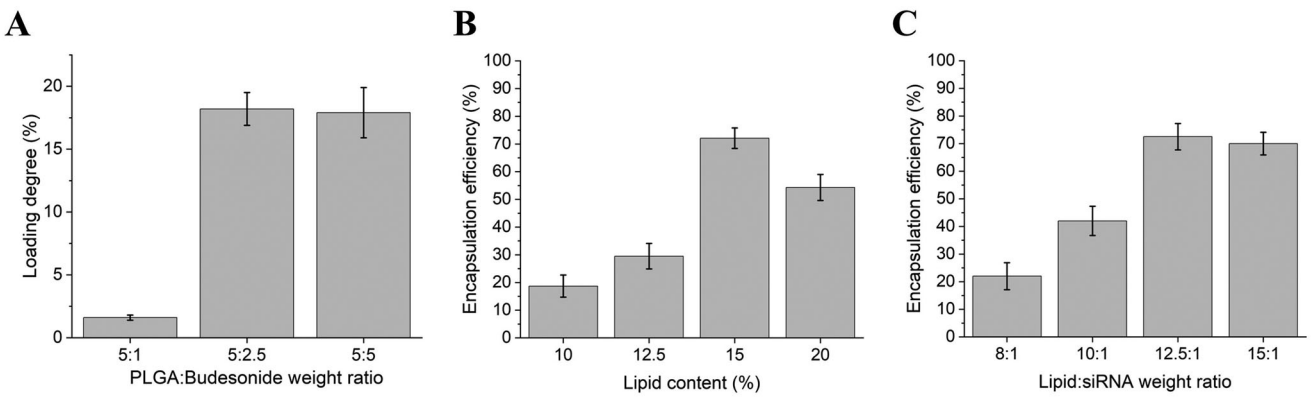

Figure 3. Quantification of loading degree (LD) of BUD and eGFP-siRNA encapsulation efficiency (EE) in LPNs. A) LD of BUD into LPNs upon variation of the initial amount of BUD added. eGFP-siRNA EE into LPNs upon variation of B) the lipid content and C) the lipid:siRNA weight ratio. Values are represented as the mean ± s.d. ($n \geq 3$).

on the number of potential hydrophobic interactions between the PLGA core and the drug and the relative saturation of the NP hydrophobic compartment.[49]

The eGFP-siRNA is a model siRNA commonly used for the optimization of formulations that can serve as platform for the delivery of different siRNAs. In previous works based on the optimization of siRNA-loaded lipid NPs, the lipid content (percentage of lipids in the formulation with respect to the total solid content) and the lipid:siRNA weight ratio have been identified as critical parameters for efficient siRNA complexation.[6,50] Herein, these formulation parameters were optimized based on the EE data.[51] For quantifying the EE of siRNA in LPNs, the Ribogreen assay was used, which is the most frequently used fluorescent-based assay in the lipid NPs field.[52] The advantage of this assay is that it allows to indirectly determine the amount of siRNA that is encapsulated in the lipid shell and not adsorbed to the surface, where it is exposed to chemical and enzymatic degradation.[28] The external calibration curves for this assay were constructed in TE buffer and Triton X-100 1% (w/v) (Figure S3, Supporting Information). By diluting the nanoparticles in TE buffer, only the siRNA outside of the NPs (either non-complexed or surface adsorbed) is quantified. By diluting the NPs in Triton X-100 1% (w/v), the lipid shell is dissolved and the encapsulated siRNA is released, so the total siRNA (the one outside and the one inside) is quantified. By subtracting these two amounts, the encapsulated siRNA is determined, and therefore the dose of NPs needed for gene silencing can be better estimated.

For optimization purposes, the eGFP-siRNA encapsulation efficiency was measured upon variation of the lipid content at levels 10%, 12.5%, 15%, and 20%, keeping the lipid:siRNA weight ratio constant at 15:1. As shown in Figure 3B, increasing the lipid content up to 15% led to an increase in the EE up to 70%, but further increasing the lipid content to 20% did not lead to higher EE, but to a lower EE of 54%. This smaller EE when the lipid content is increased to 20% can be explained by the fact that when the amount of lipids added is too high, not all lipids can interact with the PLGA core because the core is already fully wrapped by a lipid shell, so there can be formation of liposomes parallel to the hybrid LPNs. Since these liposomes can also complex some of the siRNA but they are removed in the supernatant after purification, the EE can be lower.[6]

Thus, the 15% lipid content was selected as optimal, and then the lipid:siRNA weight ratio was varied at levels 8:1, 10:1, 12.5:1, and 15:1, keeping the lipid content constant at 15%. As we can see in Figure 3C, the 8:1 weight ratio led to a low EE of 15%, suggesting that there is not enough lipid in proportion to the siRNA to allow its efficient complexation. However, increasing the weight ratio to 15:1 led to the same EE obtained for the 12.5:1 weight ratio previously tested, since the EE is of 72% for the 12.5:1 weight ratio. Therefore, the 12.5:1 weight ratio was selected as optimal to avoid the unnecessary excess of lipids.

2.3. Release Studies of BUD and eGFP-siRNA from LPNs

The in vitro release profile of BUD and eGFP-siRNA from dual-loaded and single-loaded LPNs was evaluated in phosphate-buffered saline (PBS) + 1% (w/v) Poloxamer 407 at pH 7.4 and Hank's balanced salt solution–(N-[2- hydroxyethyl]piperazine-N′-[2-ethanesulfonic acid]) with 2-(N-morpholino)ethanesulfonic acid (HBSS–MES) + 1% (w/v) Poloxamer 407 adjusted to pH 5.5 to mimic the physiological pH in noninflamed and inflamed tissue, respectively. The use of poloxamer for the release studies in the buffers is aiming to solubilize BUD and enable its quantification. In addition, the release was also evaluated in the cell culture mediums of RAW 264.7 cells and THP-1 cells with their supplements, since they are the cell media used for in vitro studies. The release of the drugs loaded into LPNs was compared to the release of the free drugs to prove the capability of LPNs to protect the cargos and provide a sustained drug release.

For the release of BUD, the study was conducted for 72 h. The amount of BUD released to the supernatant was quantified after each time point using the HPLC method described in the Experimental Section, and linear calibration curves were established in the different release mediums (Figure S2, Supporting Information). The release of BUD from LPNs loaded with 2.5 and 5 mg of BUD was compared to identify changes on the release pattern based on the initial amount of drug loaded, as observed by others.[49]

As shown in **Figure 4** and Figures S4–S6 (Supporting Information), there is an overall burst release of BUD from dual-loaded BUD@siRNA@LPNs in all medium tested during the first 30

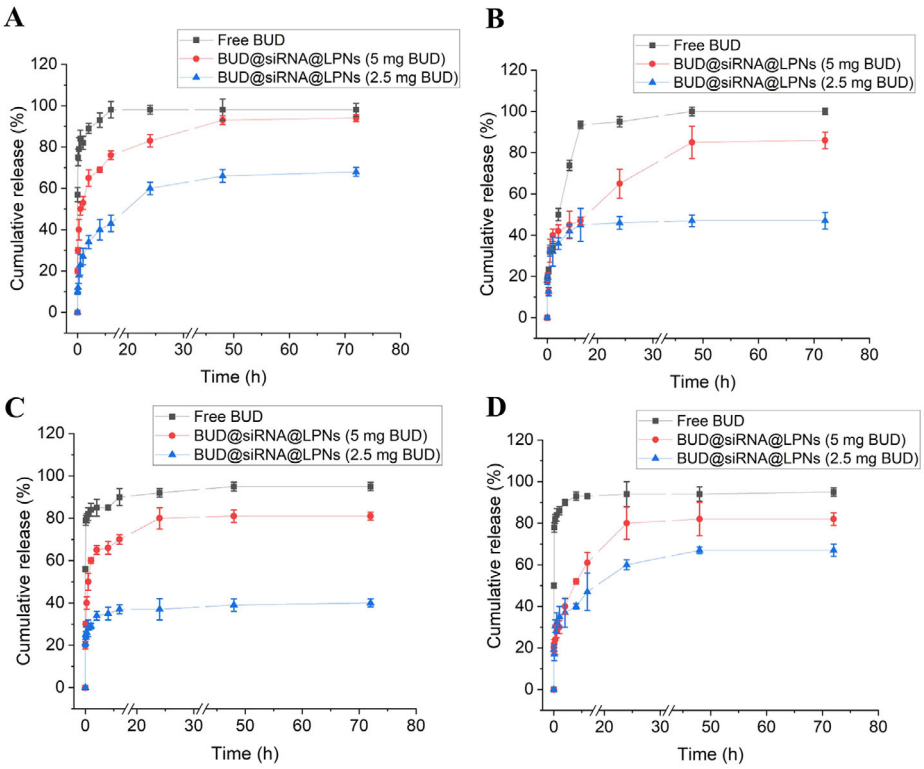

Figure 4. Release of BUD from dual-loaded BUD@siRNA@LPNs initially loaded with 2.5 and 5 mg of BUD compared to the free drug in A) PBS + 1% (w/v) Poloxamer 407 (pH 7.4), B) HBSS MES + 1% (w/v) Poloxamer 407 (pH 5.5), C) cell culture medium of RAW 264.7 cells, and D) cell culture medium of THP-1 cells at 37 °C. Data are represented as mean ± s.d. ($n \geq 3$).

min, and after this, BUD is released in a more sustained manner until the 72 h, thus demonstrating the capability of LPNs to control the release of the drug, similarly as observed in previous studies.[53,54] This burst release is remarkably more pronounced (≈60%) in PBS and DMEM cell culture medium when 5 mg is initially loaded into the LPNs compared to LPNs loaded with 2.5 mg BUD, in which a maximum of 30% burst release is obtained (Figure S4A,C, Supporting Information). This effect can be explained because when 5 mg of BUD is initially added, the system can be already saturated with the drug and therefore some BUD can be found adsorbed to the surface of LPNs to be then released as a burst. It should also be noted that there is ≈80% of BUD released after 72 h in all media when 5 mg is initially loaded in LPNs, while only 40–60% of BUD is released in total from LPNs when 2.5 mg is initially loaded. This could be explained by the fact that when 5 mg is initially loaded, the amount of polymer and lipids is still the same, so the amount of BUD that cannot be properly encapsulated could represent the ≥20% more cumulative release observed in this case.

Conversely, in HBSS MES (pH 5.5) the burst release of BUD (5 mg per NP) is half compared to that obtained for BUD at pH 7.4 (15% vs 30%) (Figure 4B; Figure S4, Supporting Information). This may be because at lower pH, the cationic lipid is more positively charged and there may be stronger electrostatic interactions preventing the burst release of the BUD adsorbed to the LPN surface.[49] However, no remarkable differences in the total BUD released was observed at pH 7.4 versus pH 5.5 for LPNs loaded with 5 mg of BUD, which might be because the initial amount of BUD loaded is the parameter conditioning the release profile the most, regardless of the pH of the medium. Regarding the release in both cell culture medium (Figure 4C,D), the lower total cumulative release of LPNs loaded with 2.5 mg of BUD in the cell medium of RAW 264.7 cells (supplemented DMEM) may be explained by the different composition of both cell medium, i.e., the medium of RAW 264.7 cells contains DMEM and nonessential amino acids while the medium for THP-1 cells contains RPMI (Roswell Park Memorial Institute) and does not contain nonessential amino acids. Finally, the release profile of BUD from the control single-loaded BUD@LPNs did not prove any significant difference with respect to the release from the dual-loaded BUD@siRNA@LPNs, confirming that the loading or not of the siRNA in the nanosystem does not affect the release profile of BUD (Figure S6, Supporting Information). Overall, the results demonstrate the possibility to sustain the release of BUD in the relevant medium, which can ensure the release of the drug upon LPNs internalization by cells.

The release of eGFP-siRNA from dual-loaded BUD@siRNA@LPNs loaded at a 12.5:1 w/w lipid:siRNA weight ratio and 15% lipid content (optimized) was evaluated to prove the capability of LPNs to protect siRNA from degradation and to control the release until 48 h, when the release is stabilized. The Ribogreen assay was used for the quantification of the siRNA released after the different time points.

As shown in **Figure 5**A and Figure S7 (Supporting Information), there is a burst release of ≈35% of the siRNA in buffer at pH 7.4 in the first 30 min, and after this, there is a progressive

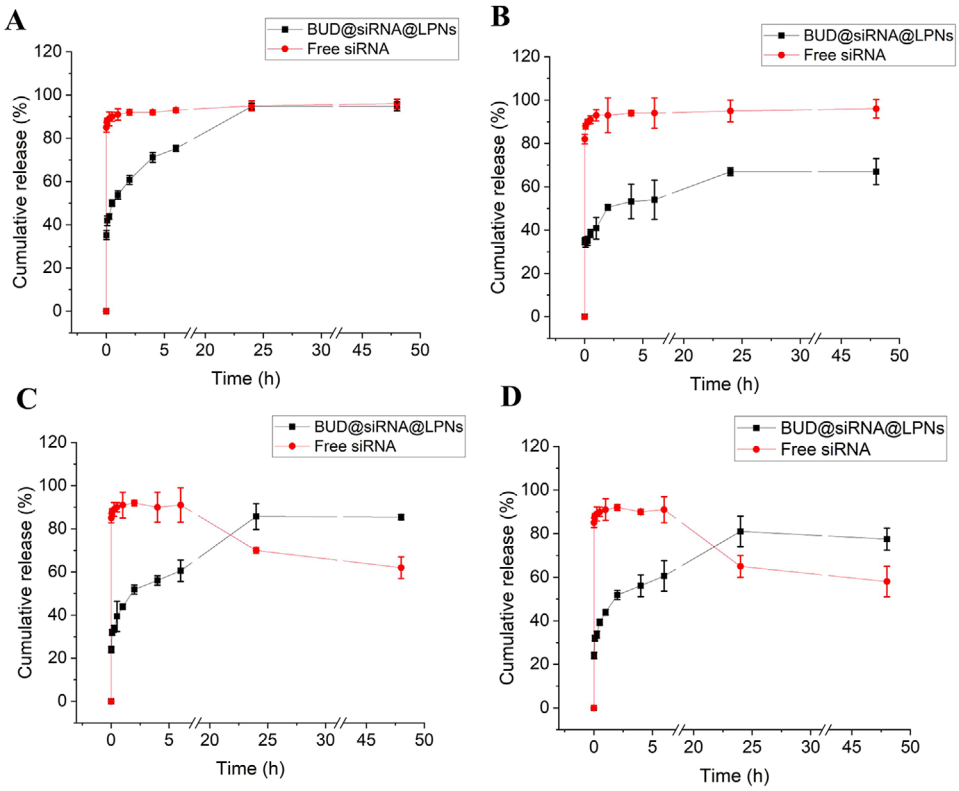

Figure 5. Release of eGFP-siRNA from dual-loaded BUD@siRNA@LPNs compared to free eGFP-siRNA in A) PBS (pH 7.4), B) HBSS–MES (pH 5.5), C) DMEM cell medium, and D) RPMI cell medium, at 37 °C. Data represented as mean ± s.d. ($n \geq 3$).

and sustained release until 24 h, when ≈90% of the siRNA is released and the plateau is reached. However, it should be noted the presence of a pH-responsive release, where in HBSS–MES (pH 5.5) the release is more sustained, since only 50% of the siRNA is released after 20 h, while more than 75% is released after that time in pH 7.4 (Figure 5A,B). In addition, after 48 h, a total of 65% of siRNA is released at pH 5.5 compared to the total of 90% released at pH 7.4. This may be due to the higher protonation of the lipidoid cKK-E12 at pH 5.5, which allows a stronger complexation of the siRNA and thus prevents a fast release at earlier time points and a complete release even at late time points. When evaluating the release in both supplemented DMEM (RAW 264.7 cells medium) and supplemented RPMI (THP-1 cells medium) (Figure 5C,D; Figure S7, Supporting Information), a similar burst release of ≈35% of siRNA in the first 30 min is observed. However, the total amount of siRNA released after 48 h is not 100%, but of ≈80%, and in RPMI medium a decay in the curve is observed in the last time point (Figure 5C,D). This can be explained by the degradation phenomena that occur when siRNA is released in the cell medium, which contains proteins that can degrade the siRNA, thus hampering its detection by the Ribogreen reagent. The degradation of the siRNA is confirmed by the release curve of the free siRNA, where we can observe a decrease in the amount of siRNA quantified after 6 h, compared to the release curves of free siRNA in buffer. Additionally, the release of siRNA from single-loaded siRNA@LPNs was measured as control, but no significant differences were observed in comparison with the release profile obtained in the dual-loaded BUD@siRNA@LPNs, confirming that the presence or absence of BUD does not affect the release of siRNA from the nanosystem (Figure S8, Supporting Information). Overall, the siRNA release profiles confirm that LPNs can protect the loaded siRNA and control the release with respect to the release of the free drug, ensuring the siRNA will be released after LPNs internalization in intact state.

2.4. Cytotoxicity Studies

The cytocompatibility of the BUD@siRNA@LPNs versus BUD@PLGA NPs was evaluated in order to prove that the coating of the PLGA core with the lipid shell does not affect the safety of the nanosystem. The cytotoxicity study was conducted in RAW 264.7 murine macrophages and human THP-1 cells differentiated to the M0 phenotype with phorbol 12-myristate 13-acetate (PMA), which are the macrophage cell lines used as model for this work to prove the suitability of LPNs as platform for drug delivery to macrophages. The cytotoxicity was evaluated using the CellTiter-Glo luminescence assay, which allows to quantify the proliferation rate of cells based on the quantification of adenosin triphosphate (ATP).[31] Cytotoxicity was determined after incubation of NPs for 24 and 48 h. The time points were chosen according to the sustained release of the drugs and the incubation time of NPs in uptake and transfection efficiency studies. Increasing the NPs' concentrations was tested to study their possible dose effect on the biosafety of LPNs.

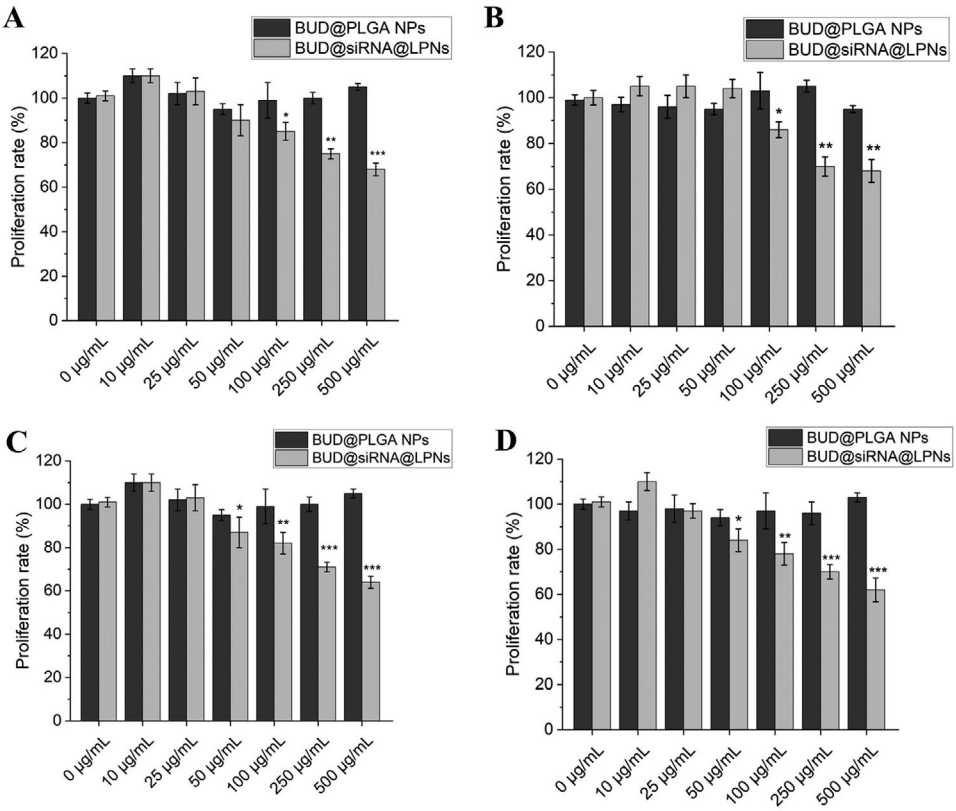

Figure 6. Cell viability of drug-loaded PLGA NPs versus LPNs. Cytocompatibility studies were conducted to assess the safety of the produced NPs on both murine RAW 264.7 cells and human THP-1 cells differentiated to M0 phenotype with PMA. A,B) Cell viability in RAW 264.7 cells after 24 and 48 h incubation, respectively. C,D) Cell viability in THP-1 cells after 24 and 48 h incubation, respectively. Results are normalized to untreated control and values are represented as mean ± s.d ($n = 3$). A one-way ANOVA followed by a Tukey–Kramer post hoc test was used for the statistical analysis. The significance levels of the differences were set at the probabilities of $*p < 0.05$, $**p < 0.01$, and $***p < 0.001$ for comparing BUD@PLGA NPs versus BUD@siRNA@LPNs.

As shown in **Figure 6**, BUD@PLGA NPs have a good biocompatibility profile as demonstrated by the absence of any cytotoxic effects on cell proliferation rate at the different tested NPs concentrations. Furthermore BUD@siRNA@LPNs demonstrated a good cytotoxic profile up to a concentration of 100 μg mL^{-1} in both cell lines after both 24 and 48 h of incubation. These results demonstrate a good biosafety profile of LPNs, similar to other studies with nanoformulations.[6,27,55,56] The reduction in the proliferation rate to 70% and 65% at concentrations of LPNs of 250 and 500 μg mL^{-1} is induced by cationic lipids activating proapoptotic cascades due to the interaction with the negatively charged DNA in the cell.[57] It should be noted that, in some cases, the proliferation rate goes higher than 100% after NPs incubation. This proliferative phenomenon induced by NPs has been previously described by other authors and it is based on the random experimental fluctuation and the stimulation of cell growth by the treatment, since the cell viability assay used in this study is sensitive to interferences with the energy metabolism.[58] In addition, Figure S9 of the Supporting Information shows that there is no significant difference in the proliferation rate between the control single-loaded BUD@LPNs and siRNA@LPNs compared to the dual-loaded LPNs in Figure 6. Similarly, Figure S10 of the Supporting Information shows that the empty PLGA NPs and LPNs had a similar biosafety profile without any remarkable differences with respect to the loaded NPs, in both cell lines. Moreover, the possible toxicity of BUD alone and eGFP-siRNA alone was evaluated by using BUD and the siRNA at analogous concentrations to those in the loaded NPs considering the loadings previously measured. As observed in Figures S11 and S12 of the Supporting Information, no decrease in the cell viability was observed when both cell lines were incubated with BUD and the siRNA alone, respectively.

2.5. Cell–Nanoparticles Interactions

The interaction of NPs with cells was then studied in the macrophage cell lines RAW 264.7 and the PMA-differentiated THP-1. The cell uptake of LPNs versus PLGA NPs was compared to confirm that coating conventional PLGA NPs with a lipid shell can improve NPs interaction with cells. To study the cell uptake, NPs were prepared using fluorescein isothiocyanate (FITC)-labeled PLGA. Based on the above-mentioned cytotoxicity studies, NPs were tested at a concentration of 100 μg mL^{-1} for all cell uptake studies, since this is the highest safe LPNs concentration. For quantitative uptake studies, the FITC-labeled NPs were incubated with the cells for 1, 3, 6, and 12 h, then washed and prepared for flow cytometry analysis.

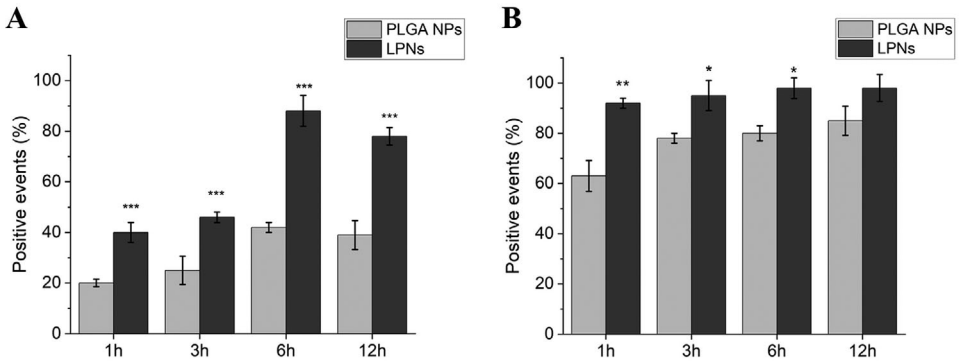

Figure 7. Quantitative NPs uptake studies comparing LPNs versus bare PLGA NPs in macrophages cell lines. Uptake studies have been carried out with both A) RAW 264.7 and B) PMA-differentiated THP-1 cell lines incubated for 1, 3, 6, and 12 h with the NPs. Values represent the positive events (%) ± s.d. ($n = 3$). A one-way ANOVA followed by a Tukey–Kramer post hoc test was used for the statistical analysis. The significance levels of the differences were set at probabilities of $*p < 0.05$, $**p < 0.01$, $***p < 0.001$ for comparison with PLGA NPs after fluorescence quenching.

For RAW 264.7 cells, we can observe a time-dependent uptake of both PLGA NPs and LPNs, where the highest cell uptake is reached at 6 h for both types of NPs (**Figure 7**A). Interestingly, the interaction of LPNs with the cells resulted in double the uptake at all time points tested compared to PLGA NPs (90% of uptake vs 40% after 6 h of incubation, respectively), demonstrating the superiority of LPNs versus the bare PLGA core when it comes to cell uptake. The lipids conforming the lipid shell coating of LPNs have fusogenic properties, and thus, can promote interaction with cell membranes and therefore cell internalization.[56,59] By contrast, PLGA NPs are negatively charged, and that leads to electrostatic repulsion that can render to lower levels of uptake, as observed by others.[27]

In THP-1 cells, the uptake kinetics is different than in RAW 264.7 cells. LPNs reach percentages of uptake of almost 100% only after 1 h, with no increase or decrease in the uptake percentages at the rest of time points (Figure 7B). In addition, PLGA NPs are taken up more efficiently than in RAW 264.7 cells, since 80% versus 40% of uptake is determined after 12 h of incubation in THP-1 versus RAW 254.7 cells, respectively. Nevertheless, LPNs are statistically significantly taken up more efficiently in all the time points between 1 and 6 h, due to the enhanced cell–nanoparticle interaction provided by the lipid coating. The overall higher and faster uptake determined for both NPs in THP-1 cells may be explained by the morphological differences between the cell lines, since RAW 264.7 cells can be cuboidal or spindle-shaped while PMA-differentiated THP-1 are spherical, and by the smaller size of RAW 264.7 cells compared to THP-1.[60] In conclusion, these results prove the superiority of LPNs to be internalized by both murine and human macrophage cell lines.

For qualitative uptake studies, confocal microscopy analysis was performed. In this case, FITC-labeled NPs were incubated with both cell lines for 6 h, the time point showing the higher percentage of cell uptake for PLGA NPs and LPNs in both cell lines. **Figure 8** shows the confocal microscopy images of LPNs after incubation with RAW 264.7 cells and PMA-differentiated THP-1 cells. Single cell images are taken by selecting one of the cells of the population in the region of interest, to better visualize the NPs inside the cells. As expected based on the quantitative data, LPNs are internalized by both cell lines with no observable differences. Nonetheless, confocal images are only representative of part of the cell population and provide only a complementary and qualitative perspective of the interactions between cells and NPs.

After confirming the high internalization of LPNs by macrophage cells, the mechanism of uptake of FITC-labeled LPNs was studied by preincubating RAW 264.7 cells and THP-1 cells for 1 h with different endocytosis inhibitors. Then, LPNs were incubated for 6 h, the cells were washed and prepared for flow cytometry analysis by quantifying FITC after trypan blue quenching, as previously described for the quantitative uptake studies. Cytochalasin D depolarizes actin filaments, and thus, was used to study the micropinocytosis and the role of actin in the endocytic process.[61] Genistein is an isoflavone, which has suppressive effects on tyrosine kinases involved in caveolin-mediated endocytosis. Sodium azide interferes with ATP production due to its ability in inhibiting cytochrome C oxidase, so it was used to study NP uptake via active transport. Methyl β-cyclodextrin is a well-known pharmacological excipient that is used to depolymerize the actin cytoskeleton, and nocodazole is used both for inhibiting the actin cytoskeleton and microtubule formation.[58]

Figure 9 shows that sodium azide is the inhibitor leading to the highest inhibition of the uptake of LPNs in both cell lines, meaning that active transport is likely one of the main mechanism controlling LPNs uptake. In RAW 264.7 cells, cytochalasin D inhibits the uptake significantly, so actin-mediated endocytosis seems to be the specific uptake mechanism for these NPs. This is in accordance with the fact that actin mechanisms are involved in phagocytosis, which characterises macrophage cells.[60] However, in THP-1 cells genistein significantly inhibits the uptake of LPNs, meaning that this type of cells also take up LPNs by caveolin-mediated endocytosis (Figure 9B).

2.6. Transfection Efficiency of BUD@siRNA@LPNs

The main requisite for functional siRNA delivery is endosomal escape and siRNA delivery to the cytoplasm. Nanocarriers composed by fusogenic lipids, such as DSPC, and cationic lipids, like cKK-E12, can enhance endosomal escape by destabilizing the endosomal membrane through electrostatic interactions and the transition of the phospholipid to the hexagonal

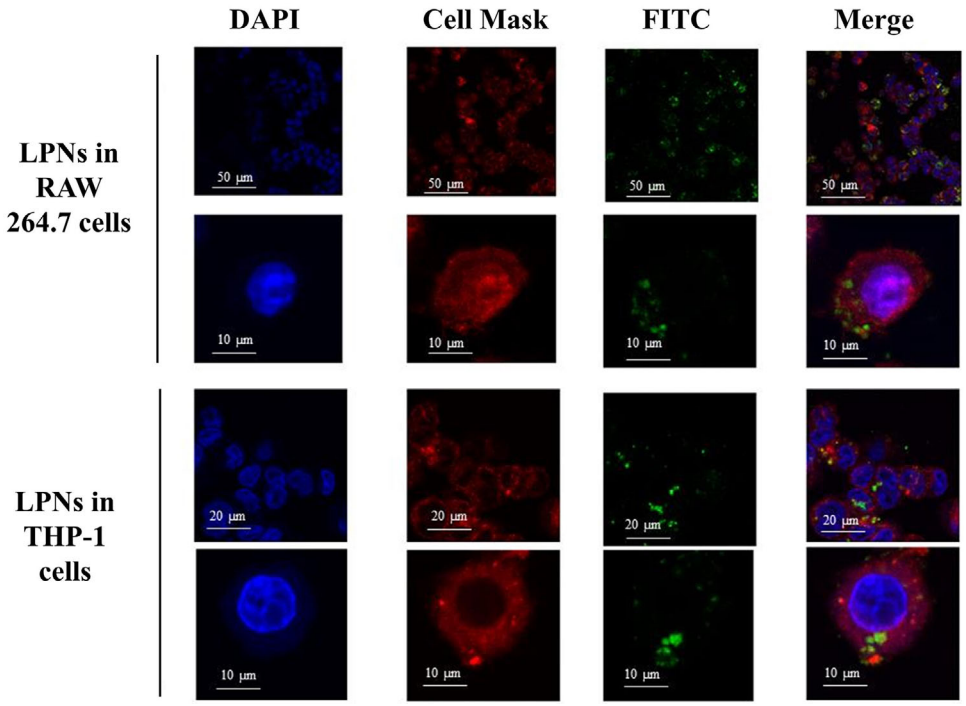

Figure 8. Qualitative uptake study of LPNs on RAW 264.7 cells and THP-1 cells using confocal fluorescence microscopy after incubation of the cells with LPNs for 6 h. The NPs were labeled with FITC (green channel), while cells were stained with 4′-6-Diamidino-2-phenylindole (DAPI) (nuclei, blue channel) and Cell Mask (cell membrane, red channel). Scale bars are shown in the images.

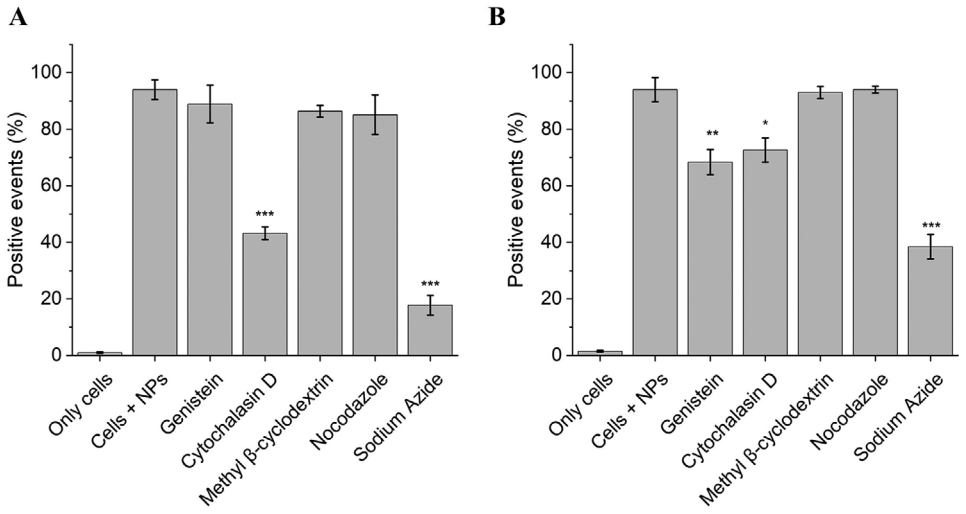

Figure 9. Uptake mechanism study of the optimized LPNs in both A) RAW 264.7 cells and B) PMA-differentiated THP-1 cells. Cells were incubated for 1 h with different compounds, each one inhibiting a different mechanism of endocytosis, then LPNs were added, and the cell uptake was evaluated after 6 h by flow cytometry. Results are represented as percentage of positive events ± s.d. ($n = 3$). A one-way ANOVA followed by a Tukey–Kramer post hoc test was used for the statistical analysis. The significance levels were set at the probabilities of $*p < 0.05$, $**p < 0.01$, and $***p < 0.001$ for comparison with the sample of cells + NPs without incubating with any inhibitor.

phase.[62] Transfection efficiency of siRNAs involves silencing of the target gene, and this can be enhanced by encapsulating the nucleic acid into a nanocarrier. When using the model eGFP-siRNA, a practical way to evaluate the transfection efficiency is by quantifying eGFP expression in eGFP-expressing cells. Herein, eGFP-expressing RAW 264.7 macrophages were treated with BUD@siRNA@LPNs using different doses of siRNA corresponding to LPNs concentrations of 2.5–200 μg mL^{-1}. Quantification of the percentage of eGFP positive ($eGFP^+$) cells was conducted by flow cytometry at 24, 48, and 72 h after incubation with BUD@siRNA@LPNs. siRNA at the dose of 0.5 μg mL^{-1} was complexed with lipofectamine as positive control, and the

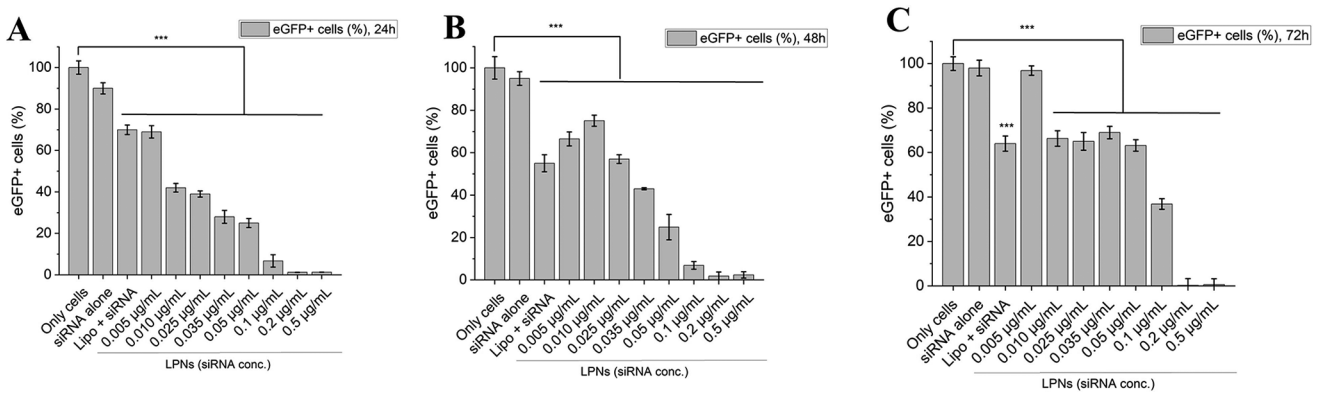

Figure 10. Transfection efficiency of dual-loaded BUD@siRNA@LPNs in eGFP-expressing RAW 264.7 cells. BUD@siRNA@LPNs were incubated at increasing concentrations for 24, 48, and 72 h, and the percentages of eGFP$^+$ cells were quantified by flow cytometry analysis. Results are represented as percentage of eGFP$^+$ cells ± s.d. ($n = 3$). A one-way ANOVA followed by a Tukey–Kramer post hoc test was used for the statistical analysis. The significance levels were set at the probabilities of $^{***}p < 0.001$ for comparison between the siRNA alone, lipofectamine + siRNA, and BUD@siRNA@LPNs versus the untreated cells.

siRNA alone and untreated cells were used as negative controls. As shown in **Figure 10**, BUD@siRNA@LPNs lead to significant reductions in the percentage of eGFP$^+$ cells, even at the lowest siRNA concentration of 0.005 μg mL^{-1}, which corresponds to LPNs concentration of 2.5 μg mL^{-1}. There is a dose-dependent decrease in the percentage of eGFP$^+$ cells at all time points, since the percentage of eGFP$^+$ cells is reduced to ≈2% when the highest dose of siRNA is used in LPNs. It should be noted that the siRNA concentration of 0.2 μg mL^{-1} leads also to ≈2% eGFP$^+$ cells and corresponds to an LPNs concentration of 100 μg mL^{-1}, which is a safe NP concentration according to the cell viability studies. Interestingly, complexes of lipofectamine and the eGFP-siRNA at the highest siRNA concentration of 0.5 μg mL^{-1} reduced the percentages of eGFP$^+$ cells to only ≈60%, which means that LPNs are much more efficient than the positive control for siRNA delivery. In addition, the maximum transfection efficiency is observed at 24 h for all the tested concentrations, which is expected because in this time point the siRNA can reach the cytoplasm allowing the silencing of the expression of the gene before the decay in the silencing effect.[44,63] Moreover, when the control single-loaded siRNA@LPNs were used in an analogous study, no significant difference in the transfection efficiency was observed compared to the dual-loaded BUD@siRNA@LPNs, suggesting that loading a small molecule in the PLGA core of the hybrid LPNs is not affecting the transfection process (Figure S13, Supporting Information). Overall, the data suggest that the optimized LPNs can be used as a platform for the efficient delivery of siRNAs to macrophages.

3. Conclusion

In this work, a new microfluidics approach was optimized for the preparation of hybrid LPNs coloaded with an anti-inflammatory small molecule drug in the PLGA core and a model siRNA in the lipid shell. The prepared LPNs showed homogenous size and colloidal stability in different media, efficient loading of BUD and eGFP-siRNA, and sustained release of the payloads. Furthermore, the LPNs were not toxic at high NP concentrations in both murine and human macrophages and displayed a higher internalization compared to the bare PLGA core in both cell lines. Finally, the transfection efficiency of LPNs was high at low NPs concentrations compared to a commercial compound. Overall, the optimized dual drug-loaded LPNs are promising candidates for the dual delivery of small molecule drugs and siRNAs to tackle complex conditions where macrophage dysregulation plays a key role.

4. Experimental Section

Materials for LPNs Preparation and Characterization: PLGA PURASORB PDLG 5004A (50/50 DL-lactide/glycolide copolymer) was kindly gifted by Corbion. FITC-labeled PLGA was obtained from Nanosoft Polymers (NC, USA). cKK-E12 was purchased from Echelon Bioscience (Salt Lake City, Utah). DSPC and cholesterol were obtained from Avanti Polar Lipids (Alabaster, AL, USA). eGFP-siRNA was obtained from Eurogentec (Seraing, Belgium) and budesonide (BUD) was purchased from TCI (Tokyo, Japan). Diethyl pyrocarbonate (DEPC) and PVA (MW, 31 000–50 000 g mol^{-1}) were purchased from Sigma-Aldrich (St. Louis, MO, USA). Quant-iT RiboGreen RNA Reagent and Tris–ethylenediamine tetra acetic acid (EDTA) buffer (10 mM Tris, 1 mM EDTA, pH 8.0) (TE Buffer) were obtained from Molecular Probes, Invitrogen (Paisley, UK).

Materials for Cell Biology Studies: RAW 264.7 cells and THP-1 cells were obtained from the American Type Culture Collection (USA). eGFP-expressing RAW 264.7 cells were purchased from Cellomics Technology (Rockville, Maryland, USA). HBSS, DMEM, RPMI 1640, fetal bovine serum (FBS), and PMA were purchased from Life Technologies Gibco, USA. CellTiter-Glo assay was purchased from Promega Corporation, USA. 10× PBS, nonessential amino acids (NEAA), L-glutamine 200 mm, penicillin (100 IU mL^{-1}), streptomycin (100 mg mL^{-1}), and trypsin (2.5%) were purchased from HyClone, GE Healthcare Lifesciences (Logan, UT, USA). Triton X-100 was purchased from Merck Millipore (Darmstadt, Germany). CellMask DeepRed, Lyso tracker, and trypsin-ethylenediamine tetra acetic acid (EDTA) were purchased from Invitrogen, USA. Lipofectamine RNAiMax was purchased from Thermo Fisher Scientific (Waltham, MA, USA).

Fabrication of Glass Capillary Microfluidics Device for Preparation of LPNs: The glass capillary nanoprecipitation chip presented a 3D coflow geometry. Borosilicate glass capillaries were assembled on a glass slide, as described elsewhere.[64] Briefly, one capillary (diameter ≈1 mm; World Precision Instruments Inc., USA) was pointed in a micropipette puller (P-97, Sutter Instrument Co., USA) to a diameter of 20 μm. This capillary was then tapered to obtain a diameter of 100 μm. The capillary was introduced and

coaxially aligned into another, bigger, capillary (inner diameter 1.10 mm; Vitrocom, USA). Transparent epoxy resin was used for sealing the connection between the capillaries. Two miscible liquids were injected separately into the microfluidic device in the same direction through polyethylene tubes attached to syringes at constant flow rates. The flow rate of the different liquids was controlled by pumps (PHD 2000, Harvard Apparatus, USA).

Preparation of Empty and Loaded LPNs: The hybrid nanoparticles without drug (LPNs) and loaded with the drugs were prepared by a coflow glass-capillary microfluidic device using an optimized two-steps microfluidics method. In the first step, the empty or BUD-loaded PLGA core was prepared. The inner and outer fluids were PLGA in acetone and aqueous PVA solution. To load BUD in the PLGA core, BUD was dissolved in the inner fluid, and the rest of the procedure was kept the same as previously described. The empty or BUD-loaded PLGA NPs were purified by ultracentrifugation at 154 324 × *g* for 30 min, washed three times and resuspended in Milli-Q water when PLGA NPs were used as control. To produce LPNs, the purified PLGA NPs were resuspended in ethanol. The suspension of empty or loaded PLGA NPs was mixed with cKK-E12:DSPC:Chol; so in the second microfluidics step, the inner phase was the ethanolic suspension of PLGA NPs with the dissolved lipids, and the outer phase was aqueous PVA solution. To make a complex between eGFP-siRNA and the cationic lipid cKK-E12, eGFP-siRNA was added in the outer phase, and the resulting empty or dual drug-loaded LPNs, named LPNs and BUD@siRNA@LPNs, respectively, were purified by ultracentrifugation at 154 324 × *g* for 30 min and were resuspended in Milli-Q water or DEPC-treated Milli-Q water when the siRNA was loaded.

Physicochemical Characterization of NPs: NPs were characterized in terms of average size (Z-average), PDI, and ζ-potential by DLS using a Zetasizer Nano ZS instrument (Malvern Panalytical Ltd., UK), as described elsewhere.[26] NP suspensions were diluted 1:50 (v/v) in prefiltered (0.22 µm) Milli-Q water and were analyzed using disposable cuvettes. The third order cumulant fitting autocorrelation function was applied to measure Z-average and PDI from scattered photon patterns with a back scattering at 173°. The photon correlation analysis was carried out with the following parameters; real refractive index 1.59, imaginary refractive index 0.0, medium refractive index 1.330, medium viscosity 1.0 mPa s, and medium dielectric constant 80.4. The Z-potential of nanoparticles was measured using the Doppler laser anemometry and hence the electrophoretic mobility, according to the Smoluchowsky constant F (Ka) of 1.5. The morphology and size homogeneity of NPs was evaluated using TEM (Jeol JEM-1400, Jeol Ltd., Japan), operating at 120 kV. For this purpose, 2 µL of a 1 mg mL^{-1} suspension of NPs was placed on a carbon coated cooper TEM grid (300 mesh; Electron Microscopy Sciences, USA). 2 µL of ammonium molibdate (1% v/v) was placed on the grid for staining the sample.[65] After 5 min, the grid was rinsed with Milli-Q water and left to dry overnight at room temperature.

Stability Studies: The stability of NPs was evaluated in 1× PBS, RAW 264.7, and THP-1 cell culture mediums and 5.4% (v/v) sucrose. Briefly, 0.6 mg of NPs was resuspended in 200 µL of Milli-Q water and immediately added to 1.6 mL of stability medium. The suspension was kept under stirring at 37 °C. Aliquots of 200 µL were taken at different time points (5 min, 15 min, 30 min, 1 h, 2 h, 6 h, and 24 h), diluted in 800 µL of Milli-Q water and measured in a disposable polystyrene cuvette (SARSTEDT AG & Co., Germany) by DLS, using a Zetasizer Nano ZS instrument (Malvern Panalytical Ltd, UK).

Quantification of BUD and eGFP-siRNA in LPNs: The amount of BUD in LPNs was quantified by Agilent 1100 HPLC (Agilent Technologies, USA), as previously described but with some modifications.[48] BUD-loaded LPNs were dissolved in 3:2 (v/v) acetonitrile:DMSO. A 200 µL sample of the dissolved NPs was centrifuged to precipitate any possible undissolved NPs, and the supernatant was analyzed. Briefly, the mobile phase was made up from acetic acid (0.5%, v/v, pH 3) and ACN (62:38, v/v) at a flow rate of 1.3 mL min^{-1} at 25 °C, and the detection wavelength was set at the wavelength of 244 nm. A Discovery C18 column (4.6 × 150 mm, 5 µm, Supelco Analytical, USA) was used as stationary phase and the injection volume of the samples was 20 µL. An external calibration curve was constructed using a concentration range between 0.5 and 500 µg mL^{-1} (Figure S2, Supporting Information). The LD of BUD in LPNs was calculated as shown in Equation (1)

$$\text{LD}\ (\%) = \frac{\text{Concentration of BUD quantified}\ (\mu\text{g mL}^{-1}) \times \text{Volume of NPs}\ (\text{mL})}{\text{Mass of NPs}\ (\mu\text{g})} \times 100 \quad (1)$$

The amount of eGFP-siRNA in LPNs was determined by using the Quant-iT RiboGreen RNA Reagent. On the one hand, the lipid shell of LPNs was dissolved using Triton X-100 (1%, v/v) to quantify the complexed and noncomplexed siRNA. LPNs were also mixed with 1× TE buffer to quantify the non-complexed siRNA and obtain the actual EE (Equation (2)). Standard solutions were also prepared in Triton X-100 (1% w/v) and in 1× TE buffer, and an external calibration curve was constructed from six concentrations (1–50 ng mL^{-1}) of eGFP-siRNA (Figure S3, Supporting Information). The Ribogreen assay was performed according to the manufacturer's protocol. Volumes of 100 µL of the diluted samples were loaded into the wells of a white 96-well plate. Then, 100 µL of the working solution of RiboGreen reagent diluted 2000 times in 1× TE buffer was added to each well, and the plate was incubated for 2–5 min in the dark. The concentration of siRNA was determined by fluorescence measurement by using a microplate reader at an excitation wavelength of 458 nm and emission wavelength of 520 nm. Each sample was assayed in triplicate. The EE was calculated as shown in Equation (2)

$$\text{EE}\ (\%) = \frac{\text{Concentration of siRNA quantified}\ (\text{ng mL}^{-1}) \times \text{Volume of sample (mL)}}{\text{Initial amount of siRNA added}\ (\text{ng})} \times 100 \quad (2)$$

In Vitro Drug Release: The drug release profile of BUD from LPNs was studied in sink conditions and compared with free BUD in PBS + 1% (w/v) Poloxamer 407 (pH 7.4), HBSS–MES + 1% (w/v) Poloxamer 407 (pH 7.4) adjusted to pH 5.5, and the cell culture mediums used for RAW 264.7 and THP-1 cells. Different initial amounts of BUD were loaded in the PLGA core (1, 2.5 mg and 5 mg). 1 mg of NPs was incubated with 5 mL of release medium to keep sink conditions. The release medium was stirred at 37 °C. At predetermined time intervals, 100 µL samples were collected and the removed volume was replaced with new release medium. The samples were centrifuged and the drug concentrations in the supernatants were quantified by HPLC as mentioned above. The release profile of eGFP-siRNA was evaluated also in the same above-mentioned media. 1 mg of LPNs was incubated with 5 mL of the corresponding release medium and samples of 100 µL were collected after each time point. These samples were centrifuged and diluted 100× for quantification of the released siRNA using the Ribogreen reagent, as previously described.

Macrophages Cell Lines and Cell Culture: RAW 264.7 cells (passages #5–#15) were cultured in DMEM supplemented with 10% (v/v) FBS, 1% (v/v) NEAA, 1% (v/v) L-glutamine, and 1% (v/v) penicillin–streptomycin. THP-1 monocytes were cultured with RPM1 medium supplemented with 10% (v/v) FBS, 1% (v/v) L-glutamine, and 1% (v/v) penicillin–streptomycin. All studies were conducted with THP-1 cells differentiated to M0 macrophages in passages #5–#15. For that, 75 nM of PMA was added when cells were seeded and left overnight. When NPs were added the day after, medium without PMA was used.

Cytotoxicity Studies: The in vitro cytotoxicity was performed in RAW 264.7 and THP-1 cells differentiated to M0 macrophages using a CellTiter-Glo luminescent cell viability assay (Promega Corp., WI, USA). The cells were seeded overnight on a 96-well plate at density of 1 × 10^4 cells per well in cell culture medium. NP suspensions were prepared in the corresponding media at different concentrations (10, 25, 50, 100, 250, and 500 µg mL^{-1}) and incubated for 24 and 48 h. A solution of 1% (v/v) of Triton X-100, cell medium, and CellTiter-Glo reagent was used as negative, positive, and blank controls, respectively. After incubation, cells were washed twice with HBSS–MES (pH 7.4). Thereafter a solution (50:50) of HBSS–MES and assay reagent (CellTiter-Glo, Promega, USA) was added to the cells for 2 min. The cell cytotoxicity was finally determined by

luminescence, by using a Varioskan Flash Multimode Reader (Thermo Fisher Scientific).

Quantitative Uptake Study: RAW 264.7 cells and THP-1 differentiated to M0 macrophage cells were seeded in 12-well plates at a density of 3×10^5 cells per well and left attaching overnight at 37 °C. The media was removed, and cells were then incubated with 100 μg mL^{-1} of FITC-labeled NPs for 1, 3, 6, 12, and 24 h. After incubation, cells were washed twice with PBS–EDTA and detached by trypsinization. Trypsin was neutralized with cell culture medium, and cells were pelleted and washed two times with PBS-EDTA. The cells were finally dispersed in PBS–EDTA and quantitative uptake was evaluated by an Accuri C6 Plus (BD Biosciences, USA). To discard the external fluorescence, quenching was done by incubation for 5 min with trypan blue (TB; 0.005% v/v). Cells were then pelleted by centrifuging, dispersed in fresh PBS–EDTA and samples were run again. All the data were analyzed with FlowJo software (Tree Star, Inc., USA) and results were reported as percentage of positive events.

Qualitative Uptake: The qualitative intracellular uptake of NPs was evaluated by confocal microscopy with a Leica TCS SP8 STED 3X CW 3D inverted microscope (Leica Microsystems, Germany). RAW 264.7 and THP-1 cells differentiated to M0 macrophages were seeded at a cell density of 5×10^4 cells per well into 8-well chambers (Lab Tek, Thermo Fisher Scientific, USA) and let attaching overnight. After incubation, macrophages were washed twice with PBS and then stained with CellMask Deep Red (Thermo Fisher, USA). Then, cells were washed twice with PBS and cells were incubated with FITC-labeled NPs at a concentration of 100 μg mL^{-1} for 6 h. Then, fixation was done using 4% (v/v) paraformaldehyde (Sigma-Aldrich, USA), and nuclear staining using DAPI at a concentration of 2.5 μg mL^{-1} (Thermo Fisher, USA). After staining steps and fixation, cells were washed three times with PBS. Images were captured by using a 63× water objective and then processed with Leica AS software (Leica Microsystems, Germany).

Uptake Mechanism Study: The endocytosis mechanism adopted by cells to uptake LPNs was studied in both RAW 264.7 and THP-1 cells. Cells were seeded in 12-well plates at a density of 3×10^5 cells per well and left attach overnight. Cells were treated with the compounds listed in Table S5 of the Supporting Information to inhibit specific uptake pathways. Incubation with the compounds was performed for 1 h and then LPNs were added. After 6 h of incubation with the LPNs, cells were washed, detached with trypsin, dispersed in PBS–EDTA and analyzed by flow cytometry, as described above.

Transfection Efficiency of BUD@siRNA@LPNs: eGFP-expressing RAW 264.7 cells were employed for in vitro gene silencing studies. The cells were maintained in RPMI 1640 medium containing 10% (v/v) FBS (Gibco, Grand Island, NY, USA) at 37 °C and 95/5% O_2/CO_2. Upon confluence, eGFP-expressing RAW 264.7 cells were seeded in 24-well plates at a density of 20 000 cells per well and left attach overnight. Suspensions of BUD@eGFP-siRNA@LPNs in cell media were added at different concentrations (2.5, 5, 10, 15, 25, 50, 100, 200 μg mL^{-1}). Lipofectamine RNAiMAX was used as positive control at the concentration suggested by the manufacturer. After 6 h of incubation, the LPNs suspensions were removed and replaced by fresh medium. After 24, 48, and 72 h from the addition of the LPNs, cells were washed with PBS–EDTA, detached by trypsinization, washed twice with PBS–EDTA, and finally resuspended in 200 μL of PBS-EDTA. The transfection efficiency was evaluated by measuring the percentage of $eGFP^+$ cells after the different time points by flow cytometry.

Statistical Analysis: Statistical analysis was performed using a GraphPad Prism 7 (GraphPad Software, Inc., La Jolla, CA, USA). The statistical methods used to analyze the data from each experiment are described in each figure caption. In general, one-way ANOVA followed by a Tukey–Kramer post hoc test was used for the statistical analyses during the different studies.

Supporting Information

Supporting Information is available from the Wiley Online Library or from the author.

Acknowledgements

H.A.S. acknowledges financial support from the Academy of Finland (Grant No. 331151) and the UMCG Research Funds. This work received funding from the European Union's Horizon 2020 research and development programme under the Marie Skłodowska Curie grant agreement No. 955685. S.W. acknowledges the financial support from the Academy of Finland (Grant No. 331106). C.C. acknowledges financial support from Strengthening of research structures and creation of R&D "Innovation Ecosystems", "National Recovery and Resilience Plan (NRRP)", Mission 4, Component 2 Investment 1.5, funded from the European Union–NextGenerationEU – VITALITY, ECS00000041 (Grant No. D73C22000840006). The authors thank the Electron Microscopy Unit and Light Microscopy Unit, Institute of Biotechnology, University of Helsinki (supported by HiLIFE and Biocenter Finland) for electron microscope and confocal imaging.

Conflict of Interest

The authors declare no conflict of interest.

Data Availability Statement

The data that support the findings of this study are available from the corresponding author upon reasonable request.

Keywords

drug delivery, hybrid nanoparticles, macrophages, microfluidics, siRNA

Received: February 9, 2023
Revised: April 20, 2023
Published online: May 25, 2023

[1] T. A. Wynn, K. M. Vannella, in *Macrophages in Tissue Repair, Regeneration, and Fibrosis*, Vol. *44*, Cell Press, **2016**, pp. 450–462.
[2] E. Cendrowicz, Z. Sas, E. Bremer, T. P. Rygiel, *The Role of Macrophages in Cancer Development and Therapy*, Vol. *13*, MDPI, **2021**.
[3] Y. Oishi, I. Manabe, in *Macrophages in Inflammation, Repair and Regeneration*, Vol. *30*, Oxford University Press, **2018**, pp. 511–528.
[4] G. Hu, M. Guo, J. Xu, F. Wu, J. Fan, Q. Huang, G. Yang, Z. Lv, X. Wang, Y. Jin, *Nanoparticles Targeting Macrophages as Potential Clinical Therapeutic Agents against Cancer and Inflammation*, Vol. *10*, Frontiers Media S.A, **2019**.
[5] X. Zang, M. Cheng, X. Zhang, X. Chen, *J. Mater. Chem. B* **2021**, *9*, 3284.
[6] A. Lokras, A. Thakur, A. Wadhwa, K. Thanki, H. Franzyk, C. Foged, *Front. Bioeng. Biotechnol.* **2021**, *8*, 33520957.
[7] W. Tao, A. Yurdagul Jr, N. Kong, W. Li, X. Wang, A. C. Doran, C. Feng, J. Wang, M. Ariful Islam, O. C. Farokhzad, I. Tabas, J. Shi, *Sci. Transl. Med.* **2020**, *12*, 32718990.
[8] J. Shen, H. C. Kim, J. Wolfram, C. Mu, W. Zhang, H. Liu, Y. Xie, J. Mai, H. Zhang, Z. Li, M. Guevara, Z. W. Mao, H. Shen, *Nano Lett.* **2017**, *17*, 2913.
[9] M. R. Citeroni, M. C. Ciardulli, V. Russo, G. della Porta, A. Mauro, M. el Khatib, M. di Mattia, D. Galesso, C. Barbera, N. R. Forsyth, N. Maffulli, B. Barboni, *Int. J. Mol. Sci.* **2020**, *21*, 32937830.
[10] R. Garash, A. Bajpai, B. M. Marcinkiewicz, K. L. Spiller, in *Drug Delivery Strategies to Control Macrophages for Tissue Repair and Regeneration*, Vol. *241*, SAGE Publications Inc., **2016**, pp. 1054–1063.

[11] K. M. Vannella, T. A. Wynn, in *Mechanisms of Organ Injury and Repair by Macrophages*, Vol. *79*, Annual Reviews Inc., **2017**, pp. 593–617.
[12] M. Lin, L. Dong, Q. Chen, H. Xu, X. Han, R. Luo, X. Pu, S. Qi, W. Nie, M. Ma, Y. Wang, F. Gao, J. Zhang, *Front. Bioeng. Biotechnol.* **2021**, *9*.
[13] J. Y. Sunwoo, C. D. Eliasberg, C. B. Carballo, S. A. Rodeo, in *The Role of the Macrophage in Tendinopathy and Tendon Healing*>, Vol. *38*, John Wiley and Sons Inc., **2020**, pp. 1666–1675.
[14] E. F. Craparo, M. Cabibbo, C. Scialabba, G. Giammona, G. Cavallaro, *Biomacromolecules* **2022**, *23*, 3439.
[15] V. Dave, K. Tak, A. Sohgaura, A. Gupta, V. Sadhu, K. R. Reddy, in *Lipid–Polymer Hybrid Nanoparticles: Synthesis Strategies and Biomedical Applications*, Vol. *160*, Elsevier B.V., **2019**, pp. 130–142.
[16] J. Ghitman, E. I. Biru, R. Stan, H. Iovu, *Mater. Des.* **2020**, *193*, 108805.
[17] G. Chen, Y. Qian, H. Zhang, A. Ullah, X. He, Z. Zhou, H. Fenniri, J. Shen, *Advances in Cancer Theranostics Using Organic–Inorganic Hybrid Nanotechnology*, Vol. *23*, Elsevier Ltd, **2021**.
[18] N. Pardi, M. J. Hogan, F. W. Porter, D. Weissman, *Nat. Rev. Drug Discovery* **2018**, *17*, 261.
[19] B. García-Pinel, C. Porras-Alcalá, A. Ortega-Rodríguez, F. Sarabia, J. Prados, C. Melguizo, J. M. López-Romero, *Nanomaterials* **2019**, *9*, 31010180.
[20] X. Han, H. Zhang, K. Butowska, K. L. Swingle, M. G. Alameh, D. Weissman, M. J. Mitchell, *An Ionizable Lipid Toolbox for RNA Delivery*, Vol. *12*, Nature Research, **2021**.
[21] N. Kamaly, B. Yameen, J. Wu, O. C. Farokhzad, in *Degradable Controlled-Release Polymers and Polymeric Nanoparticles: Mechanisms of Controlling Drug Release*, Vol. *116*, American Chemical Society, Washington, DC **2016**, pp. 2602–2663.
[22] A. Kumari, S. K. Yadav, S. C. Yadav, *Colloids Surf., B* **2010**, *75*, 1.
[23] B. Lu, X. Lv, Y. Le, *Polymers* **2019**, *11*.
[24] A. C. Anselmo, S. Mitragotri, *Bioeng. Transl. Med.* **2019**, *4*.
[25] A. Mukherjee, A. K. Waters, P. Kalyan, A. S. Achrol, S. Kesari, V. M. Yenugonda, in *Lipid–Polymer Hybrid Nanoparticles as a Next Generation Drug Delivery Platform: State of the Art, Emerging Technologies, and Perspectives*, Vol. *14*, Dove Medical Press Ltd., **2019**, pp. 1937–1952.
[26] V. Känkänen, J. Seitsonen, H. Tuovinen, J. Ruokolainen, J. Hirvonen, V. Balasubramanian, H. A. Santos, *Int. J. Pharm.* **2020**, *590*.
[27] N. Tahir, A. Madni, A. Correia, M. Rehman, V. Balasubramanian, M. M. Khan, H. A. Santos, *Int. J. Nanomed.* **2019**, *14*, 4961.
[28] H. Elkateb, L. M. Tatham, H. Cauldbeck, E. Niezabitowska, A. Owen, S. Rannard, T. McDonald, *Int. J. Pharm.* **2020**, *588*.
[29] J. Shen, W. Zhang, R. Qi, Z. W. Mao, H. Shen, in *Engineering Functional Inorganic–Organic Hybrid Systems: Advances in siRNA Therapeutics*, Vol. *47*, Royal Society of Chemistry, London **2018**, pp. 1969–1995.
[30] F. Fontana, H. Lindstedt, A. Correia, J. Chiaro, O. K. Kari, J. Ndika, H. Alenius, J. Buck, S. Sieber, E. Mäkilä, J. Salonen, A. Urtti, V. Cerullo, J. T. Hirvonen, H. A. Santos, *Adv. Healthcare Mater.* **2020**, *9*.
[31] F. Fontana, M. A. Shahbazi, D. Liu, H. Zhang, E. Mäkilä, J. Salonen, J. T. Hirvonen, H. A. Santos, *Adv. Mater.* **2017**, *29*.
[32] F. Fontana, S. Albertini, A. Correia, M. Kemell, R. Lindgren, E. Mäkilä, J. Salonen, J. T. Hirvonen, F. Ferrari, H. A. Santos, *Adv. Funct. Mater.* **2018**, *28*.
[33] F. Fontana, M. Mori, F. Riva, E. Mäkilä, D. Liu, J. Salonen, G. Nicoletti, J. Hirvonen, C. Caramella, H. A. Santos, *ACS Appl. Mater. Interfaces* **2016**, *8*, 988.
[34] S. Wang, S. Wannasarit, P. Figueiredo, J. Li, A. Correia, B. Xia, R. Wiwattanapatapee, J. Hirvonen, D. Liu, W. Li, H. A. Santos, *Mater. Horiz.* **2020**, *7*, 1573.
[35] S. Wang, S. Wannasarit, P. Figueiredo, G. Molinaro, Y. Ding, A. Correia, L. Casettari, R. Wiwattanapatapee, J. Hirvonen, D. Liu, W. Li, H. A. Santos, *Adv. Ther.* **2021**, *4*.
[36] M. Lin, L. Dong, Q. Chen, H. Xu, X. Han, R. Luo, X. Pu, S. Qi, W. Nie, M. Ma, Y. Wang, F. Gao, J. Zhang, *Front. Bioeng. Biotechnol.* **2021**, *9*.
[37] Y. He, D. Bi, J. A. Plantinga, G. Molema, J. Bussmann, J. A. A. M. Kamps, *Pharmaceutics* **2022**, *14*, 2086.
[38] F. Fontana, M. A. Shahbazi, D. Liu, H. Zhang, E. Mäkilä, J. Salonen, J. T. Hirvonen, H. A. Santos, *Adv. Mater.* **2017**, *29*.
[39] C. B. Roces, G. Lou, N. Jain, S. Abraham, A. Thomas, G. W. Halbert, Y. Perrie, *Pharmaceutics* **2020**, *12*, 332030082.
[40] X. Cheng, R. J. Lee, in *The Role of Helper Lipids in Lipid Nanoparticles (LNPs) Designed for Oligonucleotide Delivery*, Vol. *99*, Elsevier B.V., **2016**, pp. 129–137.
[41] S. C. Semple, A. Akinc, J. Chen, A. P. Sandhu, B. L. Mui, C. K. Cho, D. W. Y. Sah, D. Stebbing, E. J. Crosley, E. Yaworski, I. M. Hafez, J. R. Dorkin, J. Qin, K. Lam, K. G. Rajeev, K. F. Wong, L. B. Jeffs, L. Nechev, M. L. Eisenhardt, M. Jayaraman, M. Kazem, M. A. Maier, M. Srinivasulu, M. J. Weinstein, Q. Chen, R. Alvarez, S. A. Barros, S. De, S. K. Klimuk, T. Borland, et al., *Nat. Biotechnol.* **2010**, *28*, 172.
[42] T. Musumeci, C. A. Ventura, I. Giannone, B. Ruozi, L. Montenegro, R. Pignatello, G. Puglisi, *Int. J. Pharm.* **2006**, *325*, 172.
[43] Y. Dong, K. T. Love, J. R. Dorkin, S. Sirirungruang, Y. Zhang, D. Chen, R. L. Bogorad, H. Yin, Y. Chen, A. J. Vegas, C. A. Alabi, G. Sahay, K. T. Olejnik, W. Wang, A. Schroeder, A. K. R. Lytton-Jean, D. J. Siegwart, A. Akinc, C. Barnes, S. A. Barros, M. Carioto, K. Fitzgerald, J. Hettinger, V. Kumar, T. I. Novobrantseva, J. Qin, W. Querbes, V. Koteliansky, R. Langer, D. G. Anderson, *Proc. Natl. Acad. Sci. USA* **2014**, *111*, 3955.
[44] F. Leuschner, P. Dutta, R. Gorbatov, T. I. Novobrantseva, J. S. Donahoe, G. Courties, K. M. Lee, J. I. Kim, J. F. Markmann, B. Marinelli, P. Panizzi, W. W. Lee, Y. Iwamoto, S. Milstein, H. Epstein-Barash, W. Cantley, J. Wong, V. Cortez-Retamozo, A. Newton, K. Love, P. Libby, M. J. Pittet, F. K. Swirski, V. Koteliansky, R. Langer, R. Weissleder, D. G. Anderson, M. Nahrendorf, *Nat. Biotechnol.* **2011**, *29*, 1005.
[45] N. d'Avanzo, C. Celia, A. Barone, M. Carafa, L. di Marzio, H. A. Santos, M. Fresta, *Immunogenicity of Polyethylene Glycol Based Nanomedicines: Mechanisms, Clinical Implications and Systematic Approach*, Vol. *3*, Blackwell Publishing Ltd, **2020**.
[46] S. Pabisch, B. Feichtenschlager, G. Kickelbick, H. Peterlik, *Chem. Phys. Lett.* **2012**, *521*, 91.
[47] T. L. Moore, L. Rodriguez-Lorenzo, V. Hirsch, S. Balog, D. Urban, C. Jud, B. Rothen-Rutishauser, M. Lattuada, A. Petri-Fink, *Chem. Soc. Rev.* **2015**, *44*, 6287.
[48] S. Wang, S. Wannasarit, P. Figueiredo, G. Molinaro, Y. Ding, A. Correia, L. Casettari, R. Wiwattanapatapee, J. Hirvonen, D. Liu, W. Li, H. A. Santos, *Adv. Ther.* **2021**, *4*, 2000058.
[49] D. Leng, K. Thanki, E. Fattal, C. Foged, M. Yang, *Int. J. Pharm.* **2018**, *548*, 740.
[50] K. Thanki, S. Papai, A. Lokras, F. Rose, E. Falkenberg, H. Franzyk, C. Foged, *Pharm. Res.* **2019**, *36*.
[51] W. Alshaer, H. Zureigat, A. al Karaki, A. Al-Kadash, L. Gharaibeh, M. M. Hatmal, A. A. A. Aljabali, A. Awidi, *Eur. J. Pharmacol.* **2021**, *905*.
[52] J. A. Kulkarni, D. Witzigmann, S. Chen, P. R. Cullis, R. van der Meel, *Acc. Chem. Res.* **2019**, *52*, 2435.
[53] H. Ali, B. Weigmann, E. M. Collnot, S. A. Khan, M. Windbergs, C. M. Lehr, *Pharm. Res.* **2016**, *33*, 1085.
[54] F. Leonard, S. Srinivasan, X. Liu, E. M. Collnot, M. Ferrari, C. M. Lehr, B. Godin, *Eur. J. Pharm. Biopharm.* **2020**, *151*, 61.
[55] C. Dormenval, A. Lokras, G. Cano-Garcia, A. Wadhwa, K. Thanki, F. Rose, A. Thakur, H. Franzyk, C. Foged, *Pharm. Res.* **2019**, *36*.
[56] M. A. A. Jansen, L. H. Klausen, K. Thanki, J. Lyngsø, J. Skov Pedersen, H. Franzyk, H. M. Nielsen, W. van Eden, M. Dong, F. Broere, C. Foged, X. Zeng, *Eur. J. Pharm. Biopharm.* **2019**, *142*, 38.
[57] H. Lv, S. Zhang, B. Wang, S. Cui, J. Yan, *J. Controlled Release* **2006**, *114*, 100.
[58] G. Torrieri, F. Fontana, P. Figueiredo, Z. Liu, M. P. A. Ferreira, V. Talman, J. P. Martins, M. Fusciello, K. Moslova, T. Teesalu, V.

Cerullo, J. Hirvonen, H. Ruskoaho, V. Balasubramanian, H. A. Santos, *Nanoscale* **2020**, *12*, 2350.

[59] K. Hadinoto, A. Sundaresan, W. S. Cheow, in *Lipid–Polymer Hybrid Nanoparticles as a New Generation Therapeutic Delivery Platform: A Review*, Vol. *85*, Elsevier B.V., **2013**, pp. 427–443.

[60] D. A. Kuhn, D. Vanhecke, B. Michen, F. Blank, P. Gehr, A. Petri-Fink, B. Rothen-Rutishauser, *Beilstein J. Nanotechnol.* **2014**, *5*, 1625.

[61] J. Lu, M. Liong, S. Sherman, T. Xia, M. Kovochich, A. E. Nel, J. I. Zink, F. Tamanoi, *Nanobiotechnology* **2007**, *3*, 89.

[62] J. A. Kulkarni, D. Witzigmann, S. Chen, P. R. Cullis, R. van der Meel, *Acc. Chem. Res.* **2019**, *52*, 2435.

[63] Y. W. Wang, N. H. Liou, J. H. Cherng, S. J. Chang, K. H. Ma, E. Fu, J. C. Liu, N. T. Dai, *J. Invest. Dermatol.* **2014**, *134*, 2016.

[64] D. Liu, S. Cito, Y. Zhang, C. F. Wang, T. M. Sikanen, H. A. Santos, *Adv. Mater.* **2015**, *27*, 2298.

[65] J. Asadi, S. Ferguson, H. Raja, C. Hacker, P. Marius, R. Ward, C. Pliotas, J. Naismith, J. Lucocq, *Micron* **2017**, *99*, 40.